The Intestinal Microbiota Modulates the Anticancer Immune Effects of Cyclophosphamide

Sophie Viaud *et al.*

Science **342**, 971 (2013);
DOI: 10.1126/science.1240537

Science (print ISSN 0036-8075; online ISSN 1095-9203) is published weekly, except the last week in December, by the American Association for the Advancement of Science, 1200 New York Avenue NW, Washington, DC 20005.

The Intestinal Microbiota Modulates the Anticancer Immune Effects of Cyclophosphamide

Sophie Viaud,[1,3] Fabiana Saccheri,[1] Grégoire Mignot,[4,5] Takahiro Yamazaki,[1] Romain Daillère,[1,3] Dalil Hannani,[1] David P. Enot,[7,8] Christina Pfirschke,[9] Camilla Engblom,[9] Mikael J. Pittet,[9] Andreas Schlitzer,[10] Florent Ginhoux,[10] Lionel Apetoh,[4,5] Elisabeth Chachaty,[11] Paul-Louis Woerther,[11] Gérard Eberl,[12] Marion Bérard,[13] Chantal Ecobichon,[14,15] Dominique Clermont,[16] Chantal Bizet,[16] Valérie Gaboriau-Routhiau,[17,18] Nadine Cerf-Bensussan,[17,18] Paule Opolon,[19,20] Nadia Yessaad,[21,22,23,24] Eric Vivier,[21,22,23,24] Bernhard Ryffel,[25] Charles O. Elson,[26] Joël Doré,[17,27] Guido Kroemer,[7,8,28,29,30] Patricia Lepage,[17,27] Ivo Gomperts Boneca,[14,15] François Ghiringhelli,[4,5,6]* Laurence Zitvogel[1,2,3]*†

Cyclophosphamide is one of several clinically important cancer drugs whose therapeutic efficacy is due in part to their ability to stimulate antitumor immune responses. Studying mouse models, we demonstrate that cyclophosphamide alters the composition of microbiota in the small intestine and induces the translocation of selected species of Gram-positive bacteria into secondary lymphoid organs. There, these bacteria stimulate the generation of a specific subset of "pathogenic" T helper 17 (pT_H17) cells and memory T_H1 immune responses. Tumor-bearing mice that were germ-free or that had been treated with antibiotics to kill Gram-positive bacteria showed a reduction in pT_H17 responses, and their tumors were resistant to cyclophosphamide. Adoptive transfer of pT_H17 cells partially restored the antitumor efficacy of cyclophosphamide. These results suggest that the gut microbiota help shape the anticancer immune response.

It is well established that gut commensal bacteria profoundly shape mammalian immunity (*1*). Intestinal dysbiosis, which constitutes a disequilibrium in the bacterial ecosystem, can lead to overrepresentation of some bacteria able to promote colon carcinogenesis by favoring chronic inflammation or local immunosuppression (*2*, *3*). However, the effects of microbial dysbiosis on nongastrointestinal cancers are unknown. Anticancer chemotherapeutics often cause mucositis (a debilitating mucosal barrier injury associated with bacterial translocation) and neutropenia, two complications that require treatment with antibiotics, which in turn can result in dysbiosis (*4*, *5*). Some antineoplastic agents mediate part of their anticancer activity by stimulating anticancer immune responses (*6*). Cyclophosphamide (CTX), a prominent alkylating anticancer agent, induces immunogenic cancer cell death (*7*, *8*), subverts immunosuppressive T cells (*9*), and promotes T_H1 and T_H17 cells controlling cancer outgrowth (*10*). Here, we investigated the impact of CTX on the small intestine microbiota and its ensuing effects on the antitumor immune response.

We characterized the inflammatory status of the gut epithelial barrier 48 hours after therapy with nonmyeloablative doses of CTX or the anthracycline doxorubicin in naïve mice. Both drugs caused shortening of small intestinal villi, discontinuities of the epithelial barrier, interstitial edema, and focal accumulation of mononuclear cells in the lamina propria (LP) (Fig. 1, A and B). After chemotherapy, the numbers of goblet cells and Paneth cells were increased in villi (Fig. 1C) and crypts (Fig. 1D), respectively. The antibacterial enzyme lysozyme (but not the microbiocide peptide RegIIIγ) was up-regulated in the duodenum of CTX-treated mice (Fig. 1E). Orally administered fluorescein isothiocyanate (FITC)–dextran became detectable in the blood (*11*) 18 hours after CTX treatment, confirming an increase in intestinal permeability (Fig. 1F). Disruption of the intestinal barrier was accompanied by a significant translocation of commensal bacteria in >50% mice into mesenteric lymph nodes and spleens that was readily detectable 48 hours after CTX treatment, and less so after doxorubicin treatment (Fig. 2A). Several Gram-positive bacterial species, including *Lactobacillus johnsonii* (growing in >40% cases), *Lactobacillus murinus*, and *Enterococcus hirae*, could be cultured from these lymphoid organs (Fig. 2B).

Next, we analyzed the overall composition of the gut microbiota by high-throughput 454 pyrosequencing, followed by quantitative polymerase chain reaction (QPCR) targeting the domain bacteria and specific bacterial groups. Although CTX failed to cause a major dysbiosis at early time points (24 to 48 hours, fig. S1), CTX significantly altered the microbial composition of the small intestine (but not of the caecum) in mice bearing subcutaneous cancers (namely, metastasizing B16F10 melanomas and nonmetastasizing MCA205 sarcomas) 1 week after its administration (Fig. 2C and fig. S2). Consistent with previous reports on fecal samples from patients (*12*), CTX induced a reduction in bacterial species of the *Firmicutes* phylum (fig. S2) distributed within four genera and groups (*Clostridium* cluster *XIVa*, *Roseburia*, unclassified *Lachnospiraceae*, *Coprococcus*; table S1) in the mucosa of CTX-treated animals. QPCR was applied to determine the relative abundance (as compared to all bacteria) of targeted groups of bacteria (*Lactobacillus*, *Enterococcus*, cluster IV of the *Clostridium leptum* group) in the small intestine mucosa from CTX- versus vehicle-treated naïve and tumor-bearing mice. In tumor bearers, the total bacterial load of the small intestine at 7 days after CTX treatment, as well as the bacterial counts of the *Clostridium leptum*, was not affected (Fig. 2D). However, CTX treatment led to a reduction in the abundance of lactobacilli and enterococci (Fig. 2D). Together, these data reveal the capacity of CTX to provoke the selective translocation of distinct Gram-positive bacterial species followed by notable changes in the small intestinal microbiome.

Coinciding with dysbiosis 7 days after CTX administration, the frequencies of $CD103^+CD11b^+$ dendritic cells (fig. S3A) and T cell receptor αβ $(TCR\alpha\beta)^+CD3^+$ T cells expressing the transcription factor RORγt (fig. S3B) were significantly decreased in the LP of the small intestine (but not the colon), as revealed by flow cytometry of dissociated tissues (fig. S3B) and in situ immunofluorescence staining (fig. S3C). RORγt is required for the generation of T_H17 cells [which produce

[1]Institut National de la Santé et de la Recherche Médicale, U1015, Equipe labellisée Ligue Nationale Contre le Cancer, Institut Gustave Roussy, Villejuif, France. [2]Centre d'Investigation Clinique Biothérapie CICBT 507, Institut Gustave Roussy, Villejuif, France. [3]Université Paris-Sud, Kremlin Bicêtre, France. [4]Institut National de la Santé et de la Recherche Médicale, U866, Centre Georges François Leclerc, Dijon, France. [5]Institut National de la Santé et de la Recherche Médicale, Group Avenir, Dijon, France. [6]Faculté de Médecine, Université de Bourgogne, Dijon, France. [7]Institut National de la Santé et de la Recherche Médicale, U848, Institut Gustave Roussy, Villejuif, France. [8]Metabolomics and Cell Biology Platforms, Institut Gustave Roussy, Villejuif, France. [9]Center for Systems Biology, Massachusetts General Hospital and Harvard Medical School, Boston, MA, USA. [10]Singapore Immunology Network (SIgN), Agency for Science, Technology and Research (A* STAR), Singapore. [11]Service de Microbiologie, Institut Gustave Roussy, Villejuif, France. [12]Lymphoid Tissue Development Unit, Institut Pasteur, Paris, France. [13]Nimalerie Centrale, Institut Pasteur, Paris, France. [14]Institut Pasteur, Unit Biology and Genetics of the Bacterial Cell Wall, Paris, France. [15]Institut National de la Santé et de la Recherche Médicale, Group Avenir, Paris, France. [16]Institut Pasteur, Collection de l'Institut Pasteur, Paris, France. [17]Institut National de la Recherche Agronomique, Micalis–UMR1319, 78350 Jouy-en-Josas, France. [18]Institut National de la Santé et de la Recherche Médicale U989, Université Paris Descartes, 75730 Paris, France. [19]Institut Gustave Roussy, IFR54, Villejuif, France. [20]Institut Gustave Roussy, Institut de Recherche en Cancérologie Intégrée de Villejuif (IRCIV), Laboratoire de Pathologie Expérimentale, Villejuif, France. [21]Centre d'Immunologie de Marseille-Luminy, Aix-Marseille Université UM2, Marseille, France. [22]Institut National de la Santé et de la Recherche Médicale, UMR 1104, Marseille, France. [23]Centre National de la Recherche Scientifique, Unité Mixte de Recherche 7280, Marseille, France. [24]Assistance Publique des Hôpitaux de Marseille, Hôpital de la Conception, Marseille, France. [25]Laboratory of Molecular and Experimental Immunology and Neurogenetics, UMR 7355, CNRS-University of Orleans, Orleans, France. [26]University of Alabama at Birmingham, Birmingham, AL, USA. [27]AgroParisTech, Micalis–UMR1319, 78352 Jouy-en-Josas, France. [28]Equipe 11 labellisée Ligue contre le Cancer, Centre de Recherche des Cordeliers, Paris, France. [29]Pôle de Biologie, Hôpital Européen Georges Pompidou, Assistance Publique–Hôpitaux de Paris, Paris, France. [30]Université Paris Descartes, Paris, France.

*Joint senior authors.

†Corresponding author. E-mail: laurence.zitvogel@gustaveroussy.fr

interleukin-17 (IL-17)], and strong links between gut-residing and systemic T_H17 responses have been established in the context of autoimmune diseases affecting joints, the brain, or the pancreas (*13*–*15*). Confirming previous work (*9*, *10*), CTX induced the polarization of splenic $CD4^+$ T cells toward a T_H1 [interferon-γ (IFN-γ)–producing] and T_H17 pattern (Fig. 3A and fig. S3D). This effect was specific for CTX and was not found for doxorubicin (fig. S4). The gut microbiota was indispensable for driving the conversion of naïve $CD4^+$ T cells into IL-17 producers in response to CTX. Indeed, the ex vivo IL-17 release by TCR-stimulated splenocytes increased upon CTX treatment of specific-pathogen–free (SPF) mice, yet failed to do so in germ-free (GF) mice (Fig. 3A, left panel). Sterilization of the gut by broad-spectrum antibiotics (ATB, a combination of colistin, ampicillin, and streptomycin; fig. S5) also suppressed the CTX-stimulated secretion of IL-17 (Fig. 3A, right panel) and IFNγ by TCR-stimulated splenocytes (fig. S3D). Treatment of mice with vancomycin, an antibiotic specific for Gram-positive bacteria (*16*), also reduced the CTX-induced T_H17 conversion (Fig. 3A, right panel). In conventional SPF mice, the counts of lactobacilli and SFB measured in small intestine mucosa (Fig. 2D) positively correlated with the T_H1 and T_H17 polarization of splenocytes (Fig. 3B and fig. S3E), whereas that of *Clostridium* group IV did not (Fig. 3B). Together, these results point to a specific association between particular microbial components present in the gut lumen (and occasionally in lymphoid organs) and the polarity of T_H responses induced by CTX treatment.

CTX increased the frequency of "pathogenic" T_H17 (pT_H17) cells, which share hallmarks of T_H1 cells (nuclear expression of the transcription factor T-bet, cytoplasmic expression of IFN-γ, and surface exposure of the chemokine receptor CXCR3) and T_H17 cells (expression of RORγt, IL-17 and CCR6) (*17*, *18*), within the spleen (fig. S3F and Fig. 3C). Again, this response depended on the gut microbiota (Fig. 3C). Moreover, the increase in pT_H17 cells required expression of myeloid differentiation primary response gene 88 (*MyD88*), which signals downstream of toll-like receptors (fig. S6A) and is required for the therapeutic success of anticancer chemotherapies in several tumor models (*19*). In contrast, the two pattern recognition receptors, nucleotide-binding oligomerization domain-containing 1 (Nod1) and Nod2, were dispensable for the CTX-induced raise in splenic pT_H17 cells and for the tumor growth–retarding effects of CTX (fig. S6B). These results establish the capacity of CTX to stimulate pT_H17 cells through a complex circuitry that involves intestinal bacteria and MyD88, correlating with its anticancer effects. Beyond its general effect on the frequency of pT_H17 cells, CTX induced TCR-restricted, antigen-specific immune responses against commensal bacteria (fig. S7). Hence, we addressed whether Gram-positive bacterial species that translocated into secondary lymphoid organs in response to CTX (Fig. 2A) could polarize naïve $CD4^+$ T cells toward a T_H1 or T_H17 pattern. Both *L. johnsonii* and *E. hirae* stimulated the differentiation of naïve $CD4^+$ T cells into T_H1

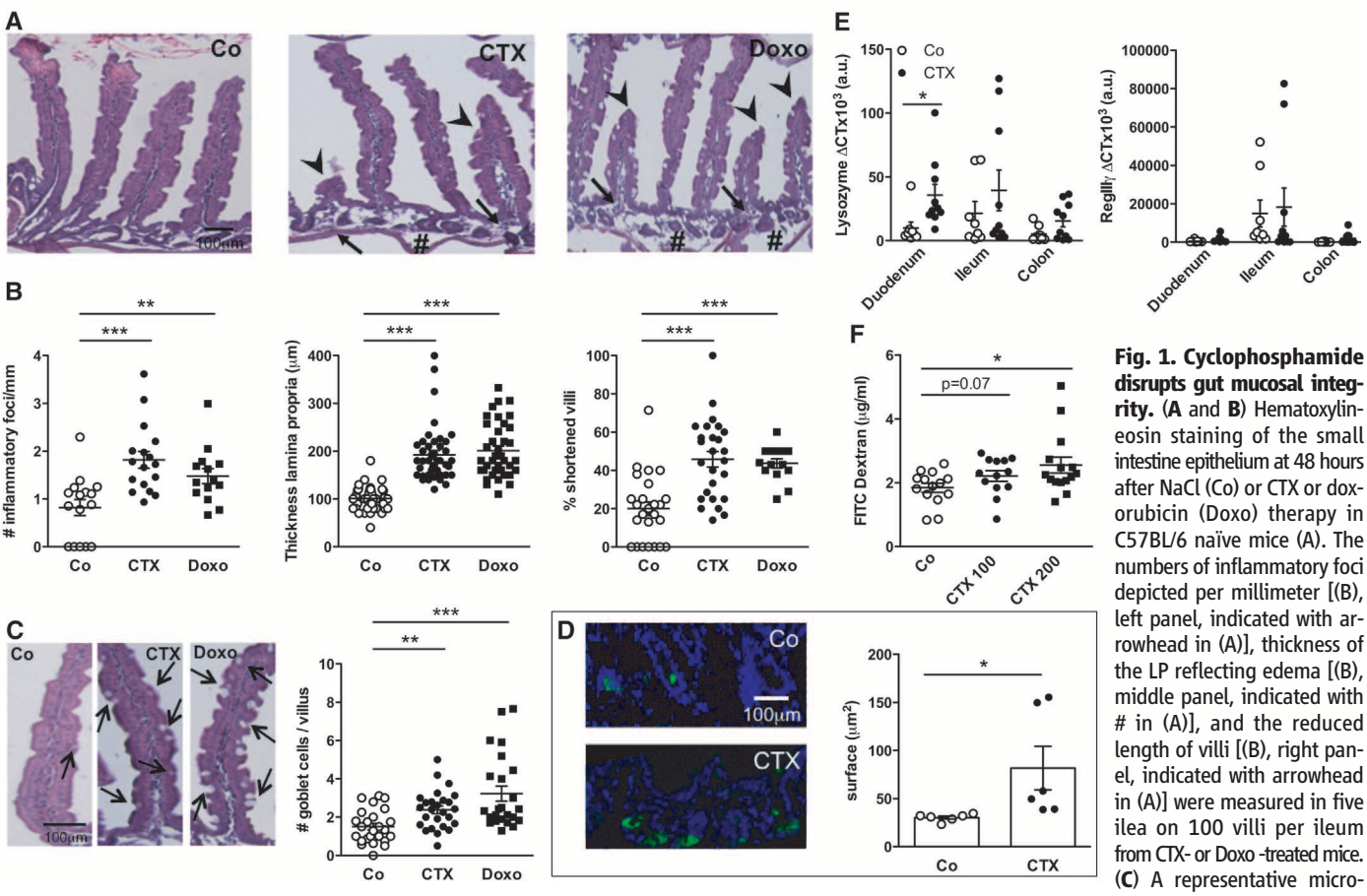

Fig. 1. Cyclophosphamide disrupts gut mucosal integrity. (**A** and **B**) Hematoxylin-eosin staining of the small intestine epithelium at 48 hours after NaCl (Co) or CTX or doxorubicin (Doxo) therapy in C57BL/6 naïve mice (A). The numbers of inflammatory foci depicted per millimeter [(B), left panel, indicated with arrowhead in (A)], thickness of the LP reflecting edema [(B), middle panel, indicated with # in (A)], and the reduced length of villi [(B), right panel, indicated with arrowhead in (A)] were measured in five ilea on 100 villi per ileum from CTX- or Doxo -treated mice. (**C**) A representative micrograph of an ileal villus containing typical mucin-containing goblet cells is shown in vehicle- and CTX- or Doxo-treated mice (left panels). The number of goblet cells per villus was enumerated in the right panel for both chemotherapy agents. (**D**) Specific staining of Paneth cells is shown in two representative immunofluorescence micrographs (left panels). The number of Paneth cells was quantified by measuring the average area of the lysozyme-positive clusters in six ilea harvested from mice treated with NaCl (Co) or CTX at 24 to 48 hours (right panel). (**E**) QPCR analyses of lysozyme M and RegIIIγ transcription levels in duodenum and ileum LP cells from mice treated with CTX at 18 hours. Means ± SEM of normalized ΔCT of three to four mice per group pooled from three independent experiments. (**F**) In vivo intestinal permeability assays measuring 4-kD FITC-dextran plasma accumulation at 18 hours after CTX treatment at two doses. Graph shows all data from four independent experiments, with each symbol representing one mouse (n = 13 to 15 mice). Data were analyzed with the Student's t test. *P < 0.05, **P < 0.01, ***P < 0.001.

and T_H17 cells in vitro, in the presence of bone marrow–derived dendritic cells, whereas toll-like receptor 4–activating purified bacterial lipopolysaccharide (LPS) or *Escherichia coli* both had a minor effect (fig. S8). Moreover, orally fed *L. johnsonii* and *E. hirae*, but neither *L. plantarum* (a bacterium that was not detected in translocation experiments, Fig. 2B) nor *L. reuteri*, facilitated the reconstitution of the pool of pT_H17 cells in the spleen of ATB-treated SPF mice (Fig. 3D). T_H1 memory responses against *L. johnsonii* were consistently detected in 50% of mice receiving CTX (Fig. 3E) but not in control mice, after in vitro restimulation of $CD4^+$ T cells with bone marrow–derived dendritic cells loaded with *L. johnsonii* (and to a lesser extent *E. hirae*, but not with other commensals or pathobionts). Taking into account that CTX-induced dysbiosis peaks at late time points (day 7), we postulate that the translocation of a specific set of Gram-positive commensal bacteria is necessary and sufficient to mediate the CTX-driven accumulation of pT_H17 cells and T_H1 bacteria-specific memory T cell responses.

Because commensal bacteria modulate intestinal and systemic immunity after CTX treatment, we further investigated the effect of antibiotics on CTX-mediated tumor growth inhibition. Long-term treatment with broad-spectrum ATB reduced the capacity of CTX to cure P815 mastocytomas established in syngenic DBA2 mice (Fig. 4A and fig. S9A). Moreover, the antitumor effects mediated by CTX against MCA205 sarcomas were reduced in GF compared with SPF mice (Fig. 4B, left and middle panels). Driven by the observations that CTX mostly induced the translocation of Gram-positive bacteria and that Gram-positive bacteria correlated with splenic T_H1/T_H17 polarization, we compared the capacity of several ATB regimens: namely, vancomycin (depleting Gram-positive bacteria) and colistin (depleting most Gram-negative bacteria) to interfere with the tumor growth–inhibitory effects of CTX. Vancomycin, and to a lesser extent colistin, compromised the antitumor efficacy of CTX against MCA205 sarcoma (Fig. 4C and fig. S9B). Using a transgenic tumor model of autochthonous lung carcinogenesis driven by oncogenic K-Ras coupled to conditional p53 deletion (*20*), we confirmed the inhibitory role of vancomycin on the anticancer efficacy of a CTX-based chemotherapeutic regimen (Fig. 4D). Vancomycin also prevented the CTX-induced accumulation of pT_H17 in the spleen (Fig. 4E) and reduced the frequencies of tumor-infiltrating $CD3^+$ T cells and T_H1 cells (Fig. 4F).

Although the feces of most SPF mice treated with ATB usually were free of cultivable bacteria (fig. S5), some mice occasionally experienced the outgrowth of *Parabacteroides distasonis*, a species reported to maintain part of the intestinal regulatory T cell repertoire and to mediate local anti-inflammatory effects (*21*–*23*). This bacterial contamination was associated with the failure of an immunogenic chemotherapy (doxorubicin) against established MCA205 sarcomas (fig. S10A). Moreover, experimental recolonization of ATB-sterilized mice with *P. distasonis* compromised the anticancer effects of doxorubicin (fig. S10B), demonstrating that gut microbial dysbiosis abrogates anticancer therapy. Finally, monoassociation of tumor-bearing GF mice with SFB, which promotes

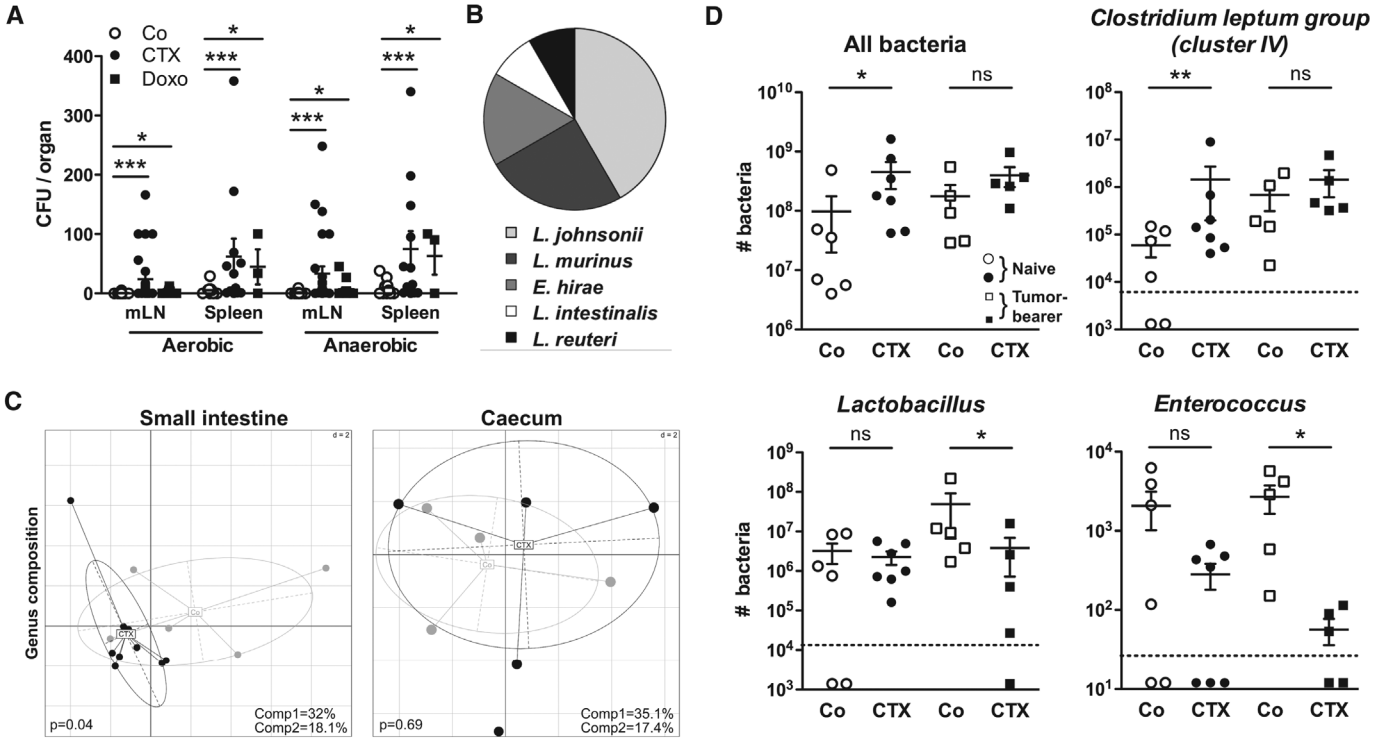

Fig. 2. Cyclophosphamide induces mucosa-associated microbial dysbiosis and bacterial translocation in secondary lymphoid organs. (**A** and **B**) At 48 hours after CTX or Doxo treatment, mesenteric lymph node (mLN) and spleen cells from naïve mice were cultivated in aerobic and anaerobic conditions, and colonies were enumerated (A) from each mouse treated with NaCl (Co) ($n = 10$ to 16 mice), CTX ($n = 12$ to 27 mice), or Doxo ($n = 3$ to 17 mice) (three to four experiments) and identified by mass spectrometry (B). In NaCl controls, attempts at bacterial identification mostly failed and yielded 67% *L. murinus* (not shown). Data were analyzed with the Student's *t* test. (**C**) The microbial composition (genus level) was analyzed by 454 pyrosequencing of the 16*S* ribosomal RNA gene from ilea and caeca of naïve mice and B16F10 tumor bearers. Principal-component analyses highlighted specific clustering of mice microbiota (each circle represents one mouse) depending on the treatment (NaCl: Co, gray circles; CTX-treated, black circles). A Monte Carlo rank test was applied to assess the significance of these clusterings. (**D**) QPCR analyses of various bacterial groups associated with small intestine mucosa were performed on CTX- or NaCl (Co)-treated, naïve, or MCA205 tumor-bearing mice. Absolute values were calculated for total bacteria, *Lactobacilli*, *Enterococci*, and *Clostridium* group IV and normalized by the dilution and weight of the sample. Standard curves were generated from serial dilutions of a known concentration of genomic DNA from each bacterial group and by plotting threshold cycles (Ct) versus bacterial quantity (colony-forming units). Points below the dotted lines were under the detection threshold. Data were analyzed with the linear model or generalized linear model. $^*P < 0.5$, $^{**}P < 0.1$, $^{***}P < 0.001$; ns, not significant.

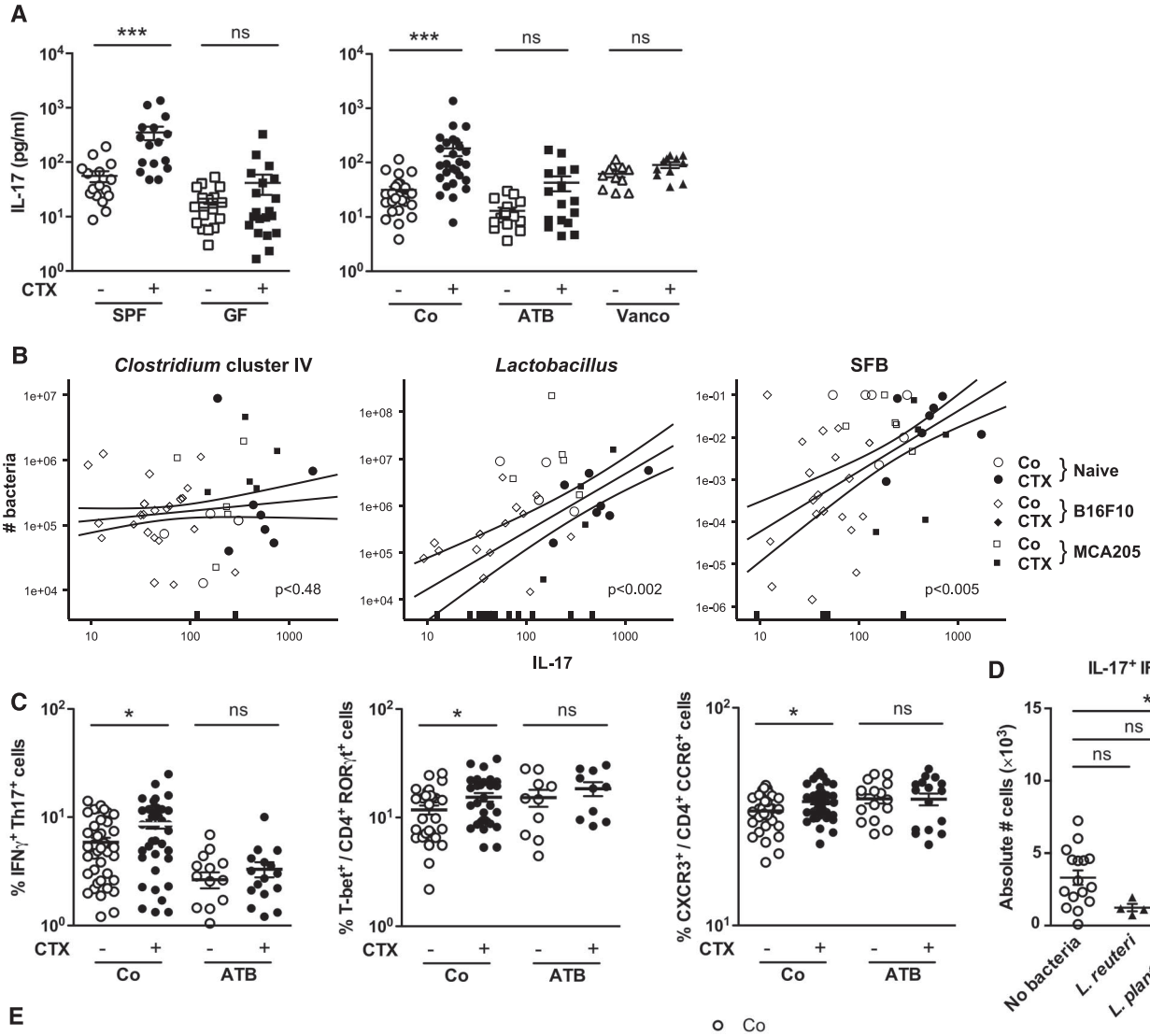

Fig. 3. CTX-induced pT$_H$17 effectors and memory T$_H$1 responses depend on gut microbiota. (**A**) Splenocytes from CTX- versus NaCl-treated animals reared in germ-free (GF) or conventional specific-pathogen–free (SPF) conditions (left panel) and treated (+) or not treated (–) with ATB or vancomycin (Vanco) (right panel) were cross-linked with antibody against CD3$^+$CD28 for 48 hours. IL-17 was measured by enzyme-linked immunosorbent assay (ELISA). Two to three experiments containing two to nine mice per group are presented, with each symbol representing one mouse. (**B**) Correlations between the quantity of specific mucosal bacterial groups and the spleen T$_H$17 signature. Each symbol represents one mouse bearing no tumor (circles), a B16F10 melanoma (diamonds), or a MCA205 sarcoma (squares); open symbols denote NaCl-treated mice and filled symbols indicate CTX-treated animals. (**C**) Intracellular analyses of splenocytes harvested from non–tumor-bearing mice after 7 days of either NaCl or CTX treatment, under a regimen of ATB or with water as control. Means ± SEM of percentages of IFN-γ$^+$ T$_H$17 cells, T-bet$^+$ cells among RORγt$^+$ CD4$^+$ T cells, and CXCR3$^+$ cells among CCR6$^+$CD4$^+$ T cells in two to eight independent experiments, with each circle representing one mouse. (**D**) Intracellular staining of total splenocytes harvested 7 days after CTX treatment from naïve mice orally reconstituted with the indicated bacterial species after ATB treatment. (**E**) Seven days after CTX or NaCl (Co) treatment, splenic CD4$^+$ T cells were restimulated ex vivo with bone-marrow dendritic cells loaded with decreasing amounts of bacteria for 24 hours. IFN-γ release, monitored by ELISA, is shown. The numbers of responder mice (based on the NaCl baseline threshold) out of the total number of mice tested is indicated (*n*). Statistical comparisons were based on the paired *t* test. Data were analyzed with either beta regression or linear model and correlation analyses from modified Kendall tau. *$P < 0.05$, ***$P < 0.001$; ns, not significant.

T_H17 cell differentiation in the LP (*1*, *13*, *14*), also had a detrimental impact on the tumor growth–inhibitory effect of CTX (Fig. 4B, right panel).

The aforementioned results highlight the association between specific CTX-induced alterations in gut microbiota, the accumulation of pT_H17 cells in the spleen, and the success of chemotherapy. To establish a direct causal link between these phenomena, we adoptively transferred T_H17

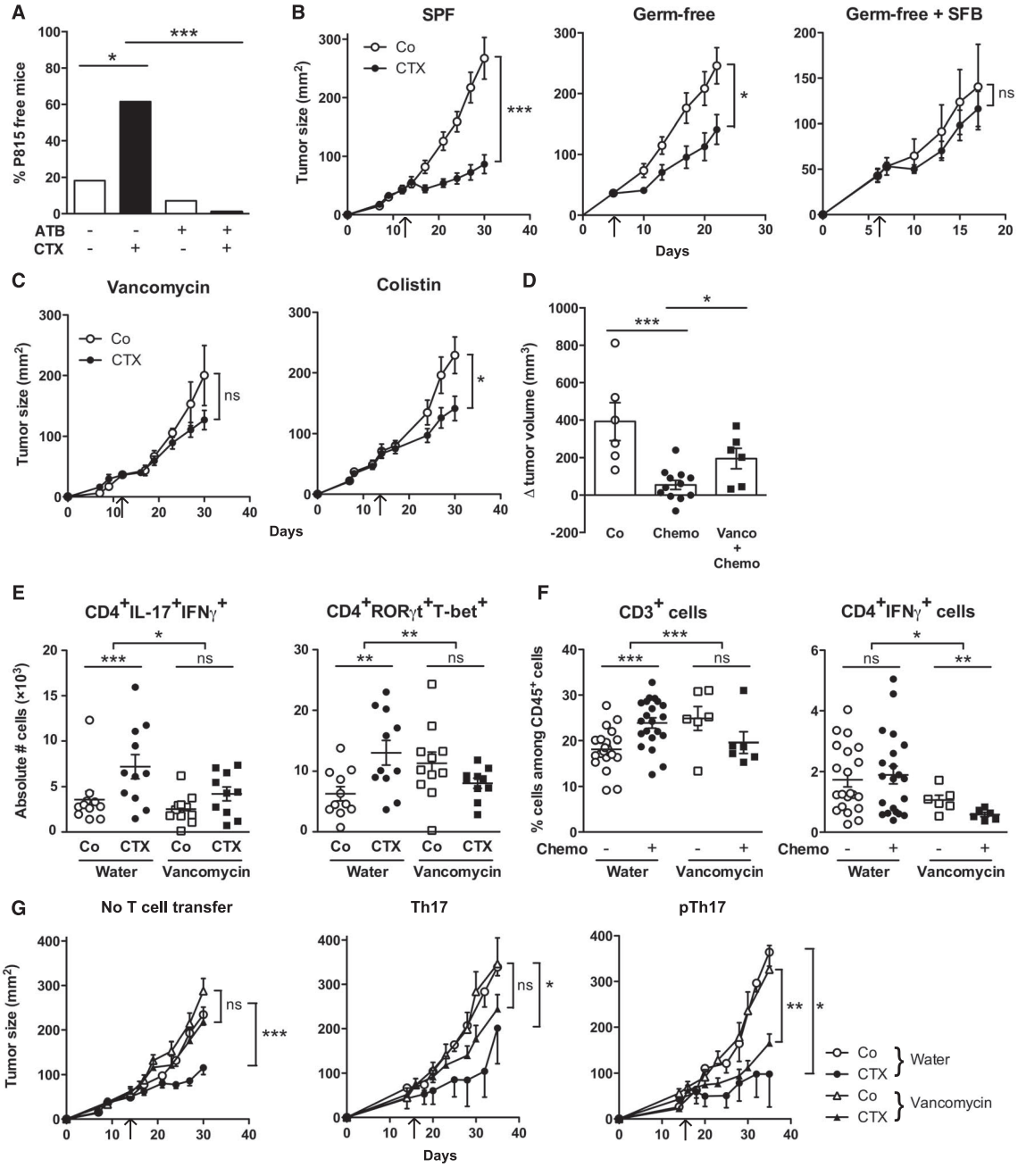

Fig. 4. Vancomycin blunts CTX-induced pT_H17 differentiation, which is mandatory for the tumoricidal activity of chemotherapy. (**A**) After a 3-week-long pretreatment with broad-spectrum ATB, DBA2 mice were inoculated with P815 mastocytomas (day 0) and treated at day 6 with CTX, and tumor growth was monitored. Tumor growth kinetics are shown in fig. S9A, and percentages of tumor-free mice at the time mice were killed are depicted for two experiments of 11 to 14 mice per group. (**B**) MCA205 sarcomas were inoculated at day 0 in specific-pathogen–free (SPF) or germ-free (GF) mice that were optionally mono-associated with segmented filamentous bacteria (SFB), treated with CTX (arrow), and monitored for growth kinetics (means ± SEM). One representative experiment ($n = 5$ to 8 mice per group) out of two or three is shown for GF mice and two pooled experiments ($n = 14$ mice per group) for SPF mice. (**C**) After a 3-week conditioning with vancomycin or colistin, C57BL/6 mice were inoculated with MCA205 sarcomas (day 0) and treated at day 12 to 15 with CTX (arrow), and tumor growth was monitored. Pooled data ($n =$ 15 to 20 mice per group) from two independent experiments are shown for colistin treatment and one representative experiment ($n = 6$ mice per group) for vancomycin treatment. (**D**) Eight-week-old KP (*KrasLSL*-G12D/WT; $p53^{Flox/Flox}$) mice received an adenovirus expressing the Cre recombinase (AdCre) by intranasal instillation to initiate lung adenocarcinoma (day 0). Vancomycin was started for a subgroup of mice (Chemo + Vanco) on day 77 after AdCre treatment. One week after the start of vancomycin, CTX-based chemotherapy was applied intraperitoneally to mice that received only chemotherapy (Chemo) or that received in parallel vancomycin (Chemo + Vanco). Mice received chemotherapy on days 84, 91, and 98. A control group was left untreated (Co). Data show the evolution of total lung tumor volumes (mean ± SEM) assessed by noninvasive imaging between days 73 and 100 in 6 to 12 mice per group. (**E**) As in Fig. 3C, we determined the number of pT_H17 cells in spleens from untreated or vancomycin-treated mice bearing established (15 to 17 days) MCA205 tumors, 7 days after CTX treatment. Each symbol represents one mouse from two pooled experiments. (**F**) Flow cytometric analyses of $CD3^+$ and $CD4^+IFN\text{-}\gamma^+$ T cells were performed by gating on $CD45^+$ live tumor-infiltrating lymphocytes extracted from day 18 established MCA205 tumors (8 days after CTX treatment) in water- or vancomycin-treated mice. Each symbol represents one mouse from up to four pooled experiments. (**G**) MCA205 tumors established in wild-type mice pretreated for 3 weeks with water or vancomycin were injected with CTX (arrow), and tumor growth was monitored. At day 7 after CTX treatment, 3 million ex vivo generated T_H17 or pT_H17 $CD4^+$ T cells were injected intravenously. Up to three experiments with 2 to 10 mice per group were pooled. Data were analyzed with either the *t* test, linear model, or generalized linear model. $^*P < 0.5$, $^{**}P < 0.1$, $^{***}P < 0.001$; ns, not significant.

or pT_H17 populations into vancomycin-treated mice and evaluated their capacity to reestablish the CTX-mediated tumor growth retardation. Ex vivo propagated pT_H17 exhibited a pattern of gene expression similar to that expressed by CTX-induced splenic $CD4^+$ T cells in vivo (fig. S11). Only pT_H17, but not T_H17 cells, could rescue the negative impact of vancomycin on the CTX-mediated therapeutic effect (Fig. 4G). These results emphasize the importance of pT_H17 cells for CTX-mediated anticancer immune responses.

Although much of the detailed molecular mechanisms governing the complex interplay between epithelial cells, gut microbiota, and intestinal immunity remain to be deciphered, the present study unveils the unsuspected impact of the intestinal flora on chemotherapy-elicited anticancer immune responses. Our data underscore new risks associated with antibiotic medication during cancer treatments, as well as the potential therapeutic utility of manipulating the gut microbiota.

References and Notes

1. L. V. Hooper, D. R. Littman, A. J. Macpherson, *Science* **336**, 1268–1273 (2012).
2. S. I. Grivennikov *et al.*, *Nature* **491**, 254–258 (2012).
3. S. Wu *et al.*, *Nat. Med.* **15**, 1016–1022 (2009).
4. M. J. van Vliet, H. J. Harmsen, E. S. de Bont, W. J. Tissing, *PLOS Pathog.* **6**, e1000879 (2010).
5. C. Ubeda *et al.*, *J. Clin. Invest.* **120**, 4332–4341 (2010).
6. G. Kroemer, L. Galluzzi, O. Kepp, L. Zitvogel, *Annu. Rev. Immunol.* **31**, 51–72 (2013).
7. A. Sistigu *et al.*, *Semin. Immunopathol.* **33**, 369–383 (2011).
8. G. Schiavoni *et al.*, *Cancer Res.* **71**, 768–778 (2011).
9. F. Ghiringhelli *et al.*, *Eur. J. Immunol.* **34**, 336–344 (2004).
10. S. Viaud *et al.*, *Cancer Res.* **71**, 661–665 (2011).
11. J. Yang, K. X. Liu, J. M. Qu, X. D. Wang, *Eur. J. Pharmacol.* **714**, 120–124 (2013).
12. J. Zwielehner *et al.*, *PLOS ONE* **6**, e28654 (2011).
13. H. J. Wu *et al.*, *Immunity* **32**, 815–827 (2010).
14. Y. K. Lee, J. S. Menezes, Y. Umesaki, S. K. Mazmanian, *Proc. Natl. Acad. Sci. U.S.A.* **108** (suppl. 1), 4615–4622 (2011).
15. L. Wen *et al.*, *Nature* **455**, 1109–1113 (2008).
16. L. B. Rice, *Am. J. Infect. Control* **34** (suppl. 1), S11–S19, discussion S64–S73 (2006).
17. Y. Lee *et al.*, *Nat. Immunol.* **13**, 991–999 (2012).
18. K. Ghoreschi *et al.*, *Nature* **467**, 967–971 (2010).
19. L. Apetoh *et al.*, *Nat. Med.* **13**, 1050–1059 (2007).
20. V. Cortez-Retamozo *et al.*, *Proc. Natl. Acad. Sci. U.S.A.* **109**, 2491–2496 (2012).
21. M. Kverka *et al.*, *Clin. Exp. Immunol.* **163**, 250–259 (2011).
22. S. K. Lathrop *et al.*, *Nature* **478**, 250–254 (2011).
23. M. B. Geuking *et al.*, *Immunity* **34**, 794–806 (2011).

Acknowledgments: We thank T. Angélique (Institut Pasteur), C. Flament, M. Vétizou (Gustave Roussy), and K. LeRoux (INRA) for technical assistance. The data reported in this manuscript are tabulated in the main paper and in the supplementary materials. This work was supported by Institut National du Cancer (INCa), la Ligue contre le cancer (LIGUE labelisée, L.Z., G.K.), SIRIC Socrates, LABEX, and PACRI Onco-Immunology, European Research Council Advanced Grant (to G.K.), and European Research Council starting grant (PGNfromSHAPEtoVIR no. 202283 to I.G.B.), and partially supported by NIH grant P01DK071176 (C.O.E.).

Supplementary Materials

www.sciencemag.org/content/342/6161/971/suppl/DC1
Materials and Methods
Supplementary Text
Figs. S1 to S12
Table S1
References (*24*–*42*)

16 September 2013; accepted 16 October 2013
10.1126/science.1240537

Substitutions Near the Receptor Binding Site Determine Major Antigenic Change During Influenza Virus Evolution

Björn F. Koel,[1] David F. Burke,[2,3] Theo M. Bestebroer,[1] Stefan van der Vliet,[1] Gerben C. M. Zondag,[4,5] Gaby Vervaet,[1] Eugene Skepner,[2,3] Nicola S. Lewis,[2,3] Monique I. J. Spronken,[1] Colin A. Russell,[3,6] Mikhail Y. Eropkin,[7] Aeron C. Hurt,[8] Ian G. Barr,[8] Jan C. de Jong,[1] Guus F. Rimmelzwaan,[1] Albert D. M. E. Osterhaus,[1] Ron A. M. Fouchier,[1]* Derek J. Smith[1,2,3,9]*

The molecular basis of antigenic drift was determined for the hemagglutinin (HA) of human influenza A/H3N2 virus. From 1968 to 2003, antigenic change was caused mainly by single amino acid substitutions, which occurred at only seven positions in HA immediately adjacent to the receptor binding site. Most of these substitutions were involved in antigenic change more than once. Equivalent positions were responsible for the recent antigenic changes of influenza B and A/H1N1 viruses. Substitution of a single amino acid at one of these positions substantially changed the virus-specific antibody response in infected ferrets. These findings have potentially far-reaching consequences for understanding the evolutionary mechanisms that govern influenza viruses.

Influenza A/H3N2 virus is a major cause of morbidity and mortality in humans and poses a considerable economic burden (*1*, *2*). Vaccination is the primary method to reduce this public health impact. The hemagglutinin (HA) surface glycoprotein is the main component of influenza vaccines, and antibodies to HA can prevent serious illnesses (*3*). However, influenza viruses can escape from antibody-mediated neutralization by accumulating mutations in HA in a process called antigenic drift, and as a consequence influenza vaccines require frequent updates. Several recent studies have focused on the identification of conserved domains of HA as targets of virus-neutralizing antibodies to circumvent this problem (*4*–*7*). Other recent work has focused on identifying the mechanisms of antigenic drift (*8*, *9*) and on sequence-based prediction to identify positively selected codons (*10*–*13*). This research has been restricted by our limited fundamental insight into the molecular basis of antigenic evolution.

Seminal work in the 1980s identified 131 amino acid positions in five antigenic sites (A to E) on the globular head of HA as main targets for specific antibodies and suggested that antigenic drift is caused by accumulation of amino acid substitutions in these sites (*14*, *15*). This work led to the widely used heuristic that it takes at least four amino acid substitutions, spread between two or more different antigenic sites, to cause substantial antigenic change. Smith *et al.* (*16*) showed that 11 antigenic clusters of viruses emerged during the 35-year period that followed the introduction of the A/H3N2 virus in humans in 1968, each of which was subsequently replaced by viruses with distinct antigenic properties. Between 1 and 13 amino acid substitutions were associated with each of the antigenic cluster transitions. Almost all of these cluster-difference substitutions were in the antigenic sites (*16*). Here, we investigated which of these substitutions actually caused the antigenic change.

We selected a representative virus from each antigenic cluster. The HA1 subunit amino acid sequence, which comprises the globular head domain of HA including the receptor binding site (RBS), of each representative virus was identical to the consensus sequence for all strains from the respective cluster (*17*). The consensus HA genes, representing natural circulating viruses, were used to make recombinant viruses in the context of the A/Puerto Rico/8/1934 reference virus (*18*). We also produced chimeric viruses with the full HA1 or with HA1 positions 109 to 301 of each antigenic cluster consensus strain in the context of HA of the Sichuan 1987 cluster consensus virus (fig. S1). The antigenic properties of all viruses were analyzed in hemagglutination inhibition (HI) assays using a panel of 8 to 16 ferret antisera raised against A/H3N2 viruses between 1968 and 2006 (table S1). The wild-type, recombinant, and chi-

[1]Department of Viroscience, Erasmus MC, 3015GE Rotterdam, Netherlands. [2]Center for Pathogen Evolution, Department of Zoology, University of Cambridge, Cambridge CB2 3EJ, UK. [3]WHO Collaborating Centre for Modeling Evolution and Control of Emerging Infectious Diseases, University of Cambridge, Cambridge CB2 3EJ, UK. [4]BaseClear B.V., 2333CC Leiden, Netherlands. [5]Luris, Leiden University, 2333AA Leiden, Netherlands. [6]Department of Veterinary Medicine, University of Cambridge, Cambridge CB3 0ES, UK. [7]Research Institute of Influenza, 197376 St. Petersburg, Russia. [8]WHO Collaborating Centre for Reference and Research on Influenza, VIDRL, Melbourne, Victoria 3051, Australia. [9]Fogarty International Center, National Institutes of Health, Bethesda, MD 20892, USA.

*Corresponding author. E-mail: dsmith@zoo.cam.ac.uk (D.J.S.); r.fouchier@erasmusmc.nl (R.A.M.F.)